Combination Strategy of Dynamic Obstacle-Avoidance and Autonomous Tracking for Hazardous Gases Inspection Robot in Man-Machine Environment

Qing-fang Zhang
Beijing Institute of Technology https://orcid.org/0000-0002-4034-4970
Xueshan Gao (xueshan.gao@bit.edu.cn)
Beijing Institute of Technology
Bing-Qing Lan
Beijing Institute of Technology
Xiao-Long Fu
Xi'an Modern Chemistry Research Institute
Jing-Ye Li
Beijing Institute of Technology

Original Article

Keywords: Dynamic obstacle avoidance, Hazardous gas detection method, Kinematics analysis, Fuzzy-PID control, Man-machine environment

Posted Date: January 9th, 2021

DOI: https://doi.org/10.21203/rs.3.rs-141377/v1

Title page

Combination Strategy of Dynamic Obstacle-avoidance and Autonomous Tracking for Hazardous Gases Inspection Robot in Man-Machine environment

Qing-Fang Zhang, born in 1994, is currently a PhD candidate at *Beijing Institute of Technology, China*. Her research interests include mobile robot, intelligent control and intelligent robotics.
Tel: +18801292685; E-mail: 3120195161@bit.edu.cn

Xue-Shan Gao, born in 1966, is currently a professor and a PhD candidate supervisor at *Beijing Institute of Technology, China*. His main research interests include mobile robot, intelligent robotics and medical robot. He is a senior member of *Chinese mechanical Engineering Society* (CMES) and an organizing committee chair of *IEEE International Conference on Mechatronics and Automation (ICMA) 2020*.
E-mail: xueshan.gao@bit.edu.cn

Bing-Qing Lan, born in 1994, is currently a master candidate at *Beijing Institute of Technology, China*.
E-mail: 2319605124@qq.com

Xiao-Long Fu, born in 1982, is currently a researcher at *Xi'an Modern Chemistry Research Institute, China.* His research interests include unmanned monitoring technology and materials science.
E-mail: fuxiaolong204@163.com

Jing-Ye Li, born in 1995. He received his master degree from *Beijing Institute of Technology, China*, in 2020. His research interests include mobile robot technology.
E-mail: lijingye0831@163.com

Corresponding author：Xue-Shan Gao　E-mail：xueshan.gao@bit.edu.cn

Combination Strategy of Dynamic Obstacle-avoidance and Autonomous Tracking for Hazardous Gases Inspection Robot in Man-Machine environment

Qing-Fang Zhang[1] • Xue-Shan Gao[1]* • Bing-Qing Lan[1] • Xiao-Long Fu[2] • Jing-Ye Li[1]

Received June xx, 2021; revised February xx, 2021; accepted March xx, 2021

Abstract: A variety of toxic and hazardous gases exist in many working or storage environments, and once a leak occurs, it will cause a wide range of casualties and immeasurable economic losses. To improve the timeliness and flexibility of the inspection equipment in a man-machine hybrid environment, this research provides an effective and practical method to improving the autonomous behavior strategy of robots in complex environments. The team designs a mobile inspection robot used to inspect hazardous gas which can be controlled remotely or inspect dangerous gas independently first, the robot is controlled by a host computer through a hybrid architecture control system mainly composed by Micro Controller Unit (MCU), Raspberry Pi based on Wi-Fi formed by a wireless router. The robot uses the hub motors as the driving wheels, equipped with multiple sensors and cameras to complete forward and backward, turning, possesses target tracking, obstacle avoidance and real-time image transmission functions softly. Based on the robot kinematic model built, this paper studies the interfering objects four typical behavior patterns, establishes a social force model to guide the robot behavioral decision-making under dynamic obstacles. To verify the effectiveness of the combination motion strategy, Matlab is used to establish a shared environment space, trajectory simulation of the state of human crossing behavior and encounter behavior, and the speed change trend of the mobile robot is recorded. Combines the dynamic obstacle avoidance strategy presented based on fuzzy thinking, an autonomous tracking strategy by adopting Fuzzy-PID controller is proposed, the experiments under fixed trajectory indoors verifies that when the robot deviates from the predetermined trajectory during inspection operations, the Fuzzy-PID control system can effectively help the robot return to the target trajectory, which the PTZ is stable and the video image is clear and the frame rate is more than 10 frames per second shows the good inspection performance. The results of simulation and test are similar, and the robot position error up to 10mm, the angle error up to 0.1 rad, which draws the reliability and accuracy of the inspection method,. And the robot can fast responsive, the small-scale time delay of the speed change does not affect the obstacle avoidance effectiveness, the robot and human will always maintain a sufficient safety distance to reduce the "sense of crisis" that humans towards to the robot.

Keywords: Dynamic obstacle avoidance • Hazardous gas detection method • Kinematics analysis • Fuzzy-PID control • Man-machine environment

1 Introduction

Hazardous gas leakage often causes a series of hazards to human's and equipment's safety, especially in natural gas factories, mines and chemical plants. Common hazardous gases are toxic and harmful (such as sulfur dioxide, carbon monoxide, etc.), also can be flammable and explosive (such as methane, etc.). Therefore, the detection of hazardous gases has become one of the most important problems which need to be solved urgently in the field of safety emergency and industrial production. With the development of robots, in factories, buildings and even homes more and more robots can be seen in the court. Among them, mobile robot has become the focus of scholars at home and abroad [1–3].

Dynamic obstacle avoidance technology is one of the important technologies for the mobile robot to realize the autonomous inspection function [4–5]. As an important manifestation of the degree of robot intelligence, it is always a difficult point in robotics research filed. Obstacle status information collection and obstacle avoidance strategies are key issues in the realization of obstacle avoidance technology.

The common algorithms of traditional obstacle avoidance algorithms include Artificial Potential Field (APF) [6],

✉ Xue-Shan Gao
xueshan.gao@bit.edu.cn

[1] Beijing Institute of Technology, Beijing 100081, China

[2] Xi'an Modern Chemistry Research Institute, Xi'an 710065, China

Essential Visibility Graph (EVG) [7], Vector Field Histogram (VFH) [8] and fuzzy logic control et al. [9–11]. In the 1980s, Khatib O [12] proposed an artificial potential field method based on a virtual force field. The planned path generated by it is relatively smooth and the obstacle avoidance effect is good. However, when the gravitation and repulsion are equal, it will fall into a local optimal solution and produce concussion route [13]. The vector field histogram proposed by Janet J et al. [14] in the 1990s has high requirements for data storage, which requires the use of sensors to collect data in advance, and the reliability of obstacle avoidance is strictly affected by sensor performance [15]. In order to avoid the original defects of the artificial potential field method, Borenstein et al. [16] proposed the VFH vector field histogram method, which verified that the specific candidate direction can successfully guide the robot to deal with the local optimal solution problem of the pure local obstacle avoidance algorithm, but the application occasions are restricted [17]. Fuzzy logic can realize dynamic obstacle avoidance in unstructured environment [18–19]. This algorithm avoids the construction of complex motion models and environmental data models, converts accurate data into fuzzy language and formulates fuzzy rules, which can effectively reduce the pressure of data calculation and improve the efficiency of obstacle avoidance [20]. In order to improve the autonomous obstacle avoidance accuracy and tracking robustness of hazardous gas inspection mobile robots in complex man-machine indoor environments, this paper proposes an combination strategy of dynamic obstacle avoidance and autonomous tracking for hazardous gases inspection robot under a fixed trajectory to realize autonomous inspection, studies the main behavior patterns of interfering objects and establishes the social force model to guide the robot makes decisions about behaviors under dynamic obstacles. The study inputs the fuzzy variables such as man-machine distance, moving linear velocity, behavior mode, and robot speed increments into fuzzy language, makes the decision-making rules through fuzzy inference, and finally designs and implements a motion controller based on fuzzy logic.

In this research, a mobile inspection robot used to inspect hazardous gas which can be controlled remotely or inspect dangerous gas independently is designed and an autonomous tracking strategy combined with dynamic obstacle avoidance strategy and is presented. The research includes four main aspects: 1) introduce robot mechanical structure and composition; 2) build the robot kinematics model; 3) design the robot control system; 4) explain the robot motion strategies. In section 5, based on fuzzy thinking, the team studies the interfering objects main behavior patterns, establishes a social force model and designs fuzzy control rules to help the robot realize dynamic obstacle avoidance. Consequently, the simulations and experiment results analysis are presented in Section 6.

2 Overall Design of Mobile Inspection Robot

Taking the functionality and applicability of the robot as the starting point, the robot is mainly composed by chassis, shell, gimbal support, gimbal, two driving wheels, two driven wheels and other electronic components.

The robot overall structure schematic diagram is shown in Figure 1 and Figure 2 is the robot prototype.

The driving wheels use a hub motor, are fixed on the chassis through mounting seat, bolts and nuts. The two driven wheels form a driven universal wheel through the wheel shaft and other parts, and then installed on the chassis. A group of short support columns and a group of long support columns are installed above the chassis respectively for mounting the robot outer shell. The hub motor driver, control board, battery and other components are installed in the middle of the shell and the chassis.

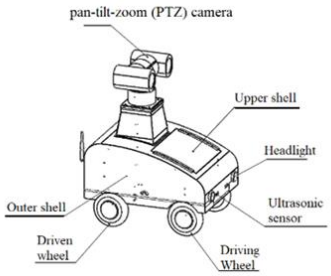

Figure 1 Schematic diagram of the robot overall structure

Figure 2 Prototype of the robot

Besides, the original components such as the power indicator, switch, emergency stop switch and charging port are installed behind the casing. Also, a grayscale sensor is installed below the chassis, four ultrasonic sensors are installed in the robot, two of them and two headlight are installed in the front of the shell, the other are installed on each side of the shell. Four supporting columns are installed in the rear of the robot where the battery is placed, and a supporting plate is installed above the supporting columns

for mounting the gimbal support, pan-tilt-zoom (PTZ) double head camera is fixed on the robot by the gimbal support and gimbal shell.

The robot can realize moving forward and backward, turning left and right through differential drive. The two driving wheels are arranged in front of the chassis and the driven wheels are arranged behind the mobile robot with gears, beam, etc. as follower are shown in Figure 3. When the two driving wheels rotate at the same speed, the robot walks straight. Turning, the two driving wheels rotate at different speeds can achieve different steering.

Figure 3 Moving mechanism of the robot

3 Kinematics Analysis of the Robot

In order to establish a robot motion model to analyze the robot kinematics, according to the robot actual application environment and the robot mechanical structure, the following assumptions are made for the robot system: 1) Assume that the robot chassis is a rigid structure, and the planes of the four wheels are perpendicular to the ground, the center of mass and centroid of each wheel overlap and are in the same plane; 2) Between the two driving wheels and the driven wheel shaft and the chassis only exist relative rotation , and the same is true between two driven wheels and the driven wheel shaft. Along the robot forward direction, the two driving wheels are the front wheels and the two driven wheels are the rear wheels; 3) Only one contact point between the four wheels and the ground, and the slight deformation of the wheels and tires is ignored; 4)The four wheels and the ground are pure rolling motion, skidding is ignored.

Set the plane global reference coordinate system {XOY}. M is the robot centroid, as the robot position reference point in the global coordinate system. The robot pose is represented by a vector $\boldsymbol{\xi}_1=[x, y, \theta]^{\mathrm{T}}$. M is at the midpoint of the two wheels，the displacement of the robot on the X and Y axes are x and y, respectively. θ is the angle difference between the global reference system and the robot reference system. The rotation speed of the left driving wheels is ω_1, the rotation speed of the right driving wheels is ω_2 and the radius of the driving wheels is r. The wheelbase of the front and rear wheels is L. The distance from the center of two front wheels to the center of mass is L_1. The distance between the rear wheel axis and the center of mass is L_2, L_3 is the distance from the rear axle to the rotating shaft. The rotation angle of the rear wheel is β. The speed at the midpoint of the two front wheels is v. Figure 4 is the robot kinematics model.

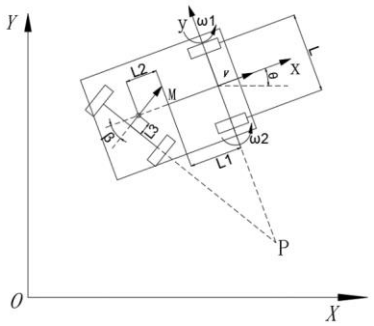

Figure 4 Kinematics model of the robot

In order to describe the robot motion state in the plane global reference system and the robot local reference system, the mapping relationship is as shown in Eq. (1).

$$\boldsymbol{\xi}_R = \boldsymbol{R}(\theta)\boldsymbol{\xi}_1, \tag{1}$$

Where, $\boldsymbol{\xi}_R$ is the robot motion vector in the local coordinate system, $\boldsymbol{R}(\theta)$ is the orthogonal rotation matrix which describes the mapping relationship between the global coordinate system and the local coordinate system.

$$\boldsymbol{R}(\theta) = \begin{bmatrix} \cos\theta & \sin\theta & 0 \\ -\sin\theta & \cos\theta & 0 \\ 0 & 0 & 1 \end{bmatrix}, \tag{2}$$

When the mobile inspection robot turns, the linear speeds v_1 and v_2 of the two driving wheels can be obtained according to the different rotation speeds of the left and right front wheels, then the midpoint linear velocity v, the angular

velocity ω of the body at this time can be got [21–22].

$$\begin{cases} v_1 = w_1 \times r \\ v_2 = w_2 \times r \end{cases}, \tag{3}$$

$$\begin{cases} v(t) = \dfrac{v_1 + v_2}{2} \\ w(t) = \dfrac{v_1 - v_2}{L} \end{cases}, \tag{4}$$

$$\dot{\xi}_1 = \begin{pmatrix} \dot{x} \\ \dot{y} \\ \dot{\theta} \end{pmatrix} = \boldsymbol{R}(\theta)^{-1} \dot{\xi}_R = \begin{bmatrix} \cos\theta & -\sin\theta & 0 \\ \sin\theta & \cos\theta & 0 \\ 0 & 0 & 1 \end{bmatrix} \begin{pmatrix} v(t) \\ \omega(t) \end{pmatrix}, \tag{5}$$

Combining Eq. (5) with Eq. (3) and Eq. (4), the kinematic model of the robot walking mechanism can be established as shown in Eq. (6).

$$\begin{aligned} \dot{\xi}_1 = \begin{pmatrix} \dot{x} \\ \dot{y} \\ \dot{\theta} \end{pmatrix} = \boldsymbol{R}(\theta)^{-1} \dot{\xi}_R &= \boldsymbol{R}(\theta)^{-1} \begin{pmatrix} \dfrac{w_1 \times r + w_2 \times r}{2} \\ 0 \\ \dfrac{w_1 \times r - w_2 \times r}{L} \end{pmatrix} \\ &= \boldsymbol{R}(\theta)^{-1} \begin{pmatrix} r & r \\ 0 & 0 \\ \dfrac{r}{L} & -\dfrac{r}{L} \end{pmatrix} \begin{pmatrix} w_1 \\ w_2 \end{pmatrix} \end{aligned}, \tag{6}$$

And the robot turning radius is:

$$R = \frac{v}{\omega} = \frac{(v_1 + v_2)L}{2(v_1 - v_2)}, \tag{7}$$

Based on the kinematics model of the robot above can design the robot control system. For this robot, the rotation angle β of the rear wheel is related to the rotation speed ratio of the left and right driving wheels.

$$\tan\beta = \frac{L_1 + L_2 + \dfrac{L_3}{\cos\beta}}{R}, \tag{8}$$

According to the Eq. (3)–(8), the indicators including the turning radius of the robot, the rotation angle β of the rear wheel and the rotation speed ratio of the left and right driving wheels can be calculated as shown in Eq. (9), (10) and (11), respectively.

$$R = (1 + \frac{\omega_1}{\omega_2})L / 2(\frac{\omega_1}{\omega_2} - 1), \tag{9}$$

$$\tan\beta = (L_1 + L_2 + \frac{L_3}{\cos\beta}) / \frac{(1 + \dfrac{\omega_1}{\omega_2})L}{2(\dfrac{\omega_1}{\omega_2} - 1)}, \tag{10}$$

$$\frac{\omega_1}{\omega_2} = \frac{2(L_1 + L_2 + \dfrac{L_3}{\cos\beta}) + L\tan\beta}{2(L_1 + L_2 + \dfrac{L_3}{\cos\beta}) - L\tan\beta}, \tag{11}$$

The wheelbase L of this robot in Figure 4 is 438mm, L_1 is 214.25mm, L_2 is 171.75mm and L_3 is 46mm. According to the formulas above, the greater the turning angle of the rear wheel is when the robot turns, the smaller the turning radius will be.

Taking into account that the driven wheel of the robot is not a direct universal wheel but is used as a whole through the combination of two universal wheels, in order to prevent the rear wheel from colliding with other parts of the robot, two gears with gear ratio of 1: 5 are installed by meshing method to control the rotation of the rear wheel. The rotation range of the pinion is controlled between -90–90 degrees by installing a limiter. Due to factors such as gear gap and installation error, when the robot turns 90 degrees, the rotation angle of the rear wheel is approximately 20 degrees, as shown in Figure 5. Taking the data to the formulas above can calculate that the rotation speed ratio of the left and right wheels of the robot is about 1.44 and the minimum turning radius is about 1.17m.

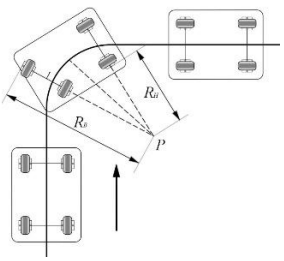

Figure 5 Schematic diagram of the robot turning motion

4 Control System Structure of the Robot

The overall structure and kinematic model of the robot has been established. This part will introduce the design of the robot corresponding control system.

Hierarchical architecture is one of the common mobile robot system structures. This structure divides the robot control system into logical and physical levels according to electrical standards. In 1970s, Scholar Saridis [23] divides the control system into organization layer, coordination layer and execution layer based on the principle of decreasing control accuracy [24]. With the rapid development of sensor systems and widespread application in robots, a classic three-tier structure of Sense-Panning-Action (SPA) layered architecture emerged [25−26]. However, the completion of each task action requires hierarchical calculation and transmission, resulting in inevitable control delay, lacking of flexibility and real-time. The behavior-based inclusive architecture can avoid long-link information transmission and improve the robot rapid response functions. The independent packaging of functions improves the robustness, stability and scalability of the system. However, due to the lack of task guidance and coordinator plan, the shortcomings such as insensitivity to information accuracy, high error rate, and lack of initiative in target tasks exposed. In order to improve the rapid responsiveness of the system and get the overall coordination and decision-making abilities, finally adopts a hybrid architecture in the overall design of the control system, a hierarchical architecture as the basic framework, and sub-systems with inclusive characteristics forms an organic fusion. The application of hybrid architecture can not only fully reflect the advantages of the above two classic architectures, but can also effectively solve the single structure control limitations.

As shown in Figure 6, the control system of the robot is mainly composed by perception layer, decision-making layer and executive layer.

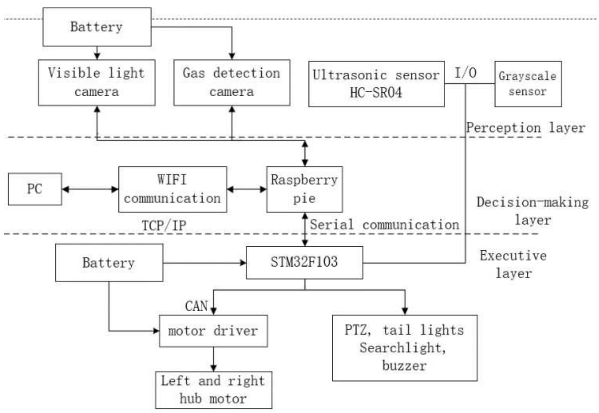

Figure 6 Structure of the robot control system

The entire robot power supply is provided by a lithium battery and a corresponding voltage conversion circuit. The perception layer is composed of sensors and cameras on the robot, which are mainly used to collect environmental information around the robot to detect hazardous gases and implement dynamic obstacle avoidance. In the perception layer, the visible light camera DS−2ZMN3007 and the infrared gas camera FLIR G200a are connected to the Raspberry Pi which is at the decision layer through network communication to detect gas leakage. Ultrasonic sensor and grayscale sensor are connected to STM32F103 through I/O port, the signal is processed through STM32F103 and then transmitted to the decision-making Raspberry Pi through the serial port.

The decision-making layer of the robot is composed by Raspberry Pi and Raspberry 4B, which are client and server, respectively. The Raspberry Pi can send and receive control commands and display these commands on terminal interface through Wi−Fi established by router. When the camera image data is collected, the image data needs to be hard coded in H.264, and compressed into H.264 format video image. In order to ensure the smoothness of the video, the frame rate of the output video image should be more than 10 frames per second. Therefore, UDP protocol is selected in the transport layer to improve the efficiency of video transmission and improve the problem of video delay. After receiving the information, the decision-making layer will process the information and send these commands to executive layer.

The executive layer mainly includes STM32F103 controller, motion control software, hub motor driver, hub motor, PTZ and other related communication modules. The microcontroller unit (MCU) STM32F103 runs the embedded system, sends the motion information of the rotation speed and displacement and uploads the sensing layer information to the upper computer through the serial communication. After receiving the corresponding instruction, the hub motor and PTZ will be droved to complete the established action.Additionally, the MCU can obtain and analyze the distance information of the ultrasonic sensor to prevent collision accidents in an emergency by internal obstacle avoidance strategy.

5 Motion Control of the Robot

5.1 Dynamic Obstacle Avoidance Strategy of the Robot

When the robot perform inspection tasks, while ensuring that the robot does not collide with interference especially humans, it should also maintain a reasonable safety range with humans to prevent humans from having a "sense of crisis". Therefore, when formulating robot inspection rules, set humans as interfering objects in the shared space.

Considering the robot target operating environment and the robot autonomous tracking strategy, adjusting the moving direction is not the best way to avoid obstacles. In order to improve safety, finally adopts fixed-point and fixed-track inspection method to obtain appropriate speed control parameters by formulating social force models and fuzzy rules that match the required environment.

5.1.1 Social Power Model

In general, each person and robot will have their own local motion targets, individual motion speeds, and accelerations in the man-machine behavior model. The following three force items should be considered in the modeling process [27]: 1) The acceleration term is the trend to reach the desired speed, F_{acc}; 2) The force term is that reflects the boundary condition of maintaining a certain distance during the interaction between human and robot, F_{int}; 3) The attractive force term is that the target to human/robot, F_{att}.

Assuming that the above three components affect pedestrian decision-making at the same time, as shown in Figure 7, quoting the traditional force superposition principle, the total effect force equation can be obtained:

$$\sum F_{total} = F_{acc} + F_{\text{int}} + F_{att}, \tag{12}$$

The social force model can predict local human motion trends, guide robot behavior strategies to ensure a communication space between robots and humans. The social space is calculated by the following Eq. (13):

$$\begin{aligned} R_{r,avoid} &= R_{\theta,avoid} + v_{r,\theta} t \\ \frac{\mathrm{d}}{\mathrm{d}t} v_{r,\theta} &= \frac{\sum F}{m} \end{aligned}, \tag{13}$$

$R_{\text{r,avoid}}$,$R_{\theta,\text{avoid}}$ are the avoidance distance of the robot and the avoidance distance of the human, respectively. As a result, the relationship between the robot kinematics model and the tendency of the interference individual can be obtained.

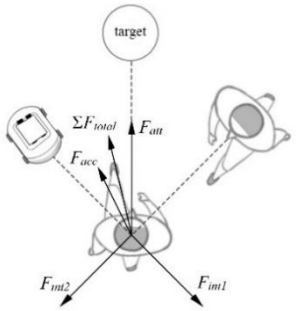

Figure 7 Social power model

5.1.2 Behavioral pattern analysis

According to the man-machine relative distance, relative motion direction, relative position and relative speed factors in the shared space environment, adopts empirical method andheuristic method to divide the behavior of human (or interfering body) into four types [28]: crossing, encountering, leading and confronting typical mode. According different typical behavior patterns, the robot follows the corresponding rules to ensure safety and does not invade sensitive areas.

1) Crossing behavior. In the man-machine coexistence scene, the crossing behavior usually appears at the intersection of the passage, which is an interfering body will cross in the forward direction of the robot. When it happens, the robot needs to judge according to the combination of the interfering body position and speed factors to determine whether to wait or pass. 2) Encountering behavior. In this passage scene, the robot and the interfering body will meet face-to-face, and the two motion directions do not affect each other, but may enter the sensitive areas of both sides. 3) Leading behavior. The interfering body appears directly in front of the robot, and both sides move in the same direction. 4) Confronting behavior. The interfering body appears directly in front of the mobile robot, but the two sides move in opposite directions.

In order to keep the robot motion range in a friendly state with humans, and not to invade individual sensitive areas, the above four types of behavior rules are designed based on the principle of no collision and no interference.

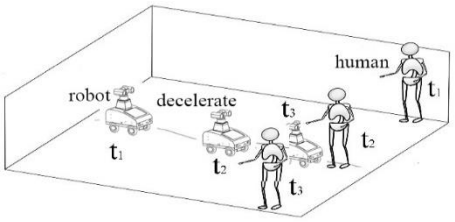

(a) Crossing behavior

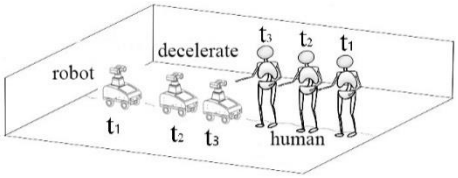

(b) Encountering behavior

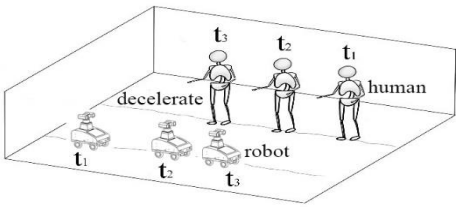

(c) Leading behavior

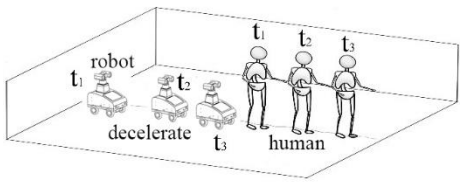

(d) Confronting behavior

Figure 8 Four type of behavior mode

5.1.3 Behavioral pattern analysis

The fuzzy logic control method is used to deal with the behavioral movement rules of the interfering objects and the robot specific strategies. Based on the above analysis of basic human behavior patterns, the robot possess the decision-making capabilities similar to humans through speed adjustment. To realize fuzzy logic control, the following three steps are required: fuzzification of input and output, fuzzy reasoning, and defuzzification of output variables.

(1) Fuzzification of input and output

In the robot dynamic obstacle avoidance control system, the input of the selected controller is the distance between man and machine, R_r, the mode of interference behavior B_i and the linear velocity of the interfering object v_i, and the output is the robot linear velocity increment Δv_i. Except for interference behavior patterns, these input/output quantities are continuous variables and their membership functions can be linearized using Gaussian functions.

When the man-machine distance is less than the robot maximum avoidance distance, $R_{r,avoid}$ at the current speed, the control signal starts to be generated. But the minimum cannot be less than the human sensitive area, and the distance from the boundary of the sensitive area to the center of the circle is R_{sen}. Divide the man-machine distance domain into {DS DE DN DF}, where DS stands for human sensitive distance, DE stands for 75% avoidance distance, DN stands for 90% avoidance distance, DF stands for maximum robot avoidance distance, and its membership function is shown in Figure 9(a). Divide the moving linear velocity domain of the interfering object into {VS VF}, and its three language variables represent "fast" and "slow", respectively. The division basis is determined according to the normal walking speed of humans. The membership function is shown in Figure 9(b). Divide the domain of the behavior mode of interference into {BS BE BL BF}, which respectively represent crossing behavior, encountering behavior, leading behavior and confronting behavior. The membership function is shown in Figure 9(c). Divide the domain of the output robot linear velocity increment into {VD VZ VI VR VT}, which represent stop in place, the original set inspection speed is 25%, 50%, 75% and 100%. The membership function is as Figure 9(d) shows.

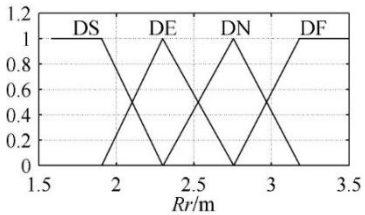

(a) Domain of man-machine distance

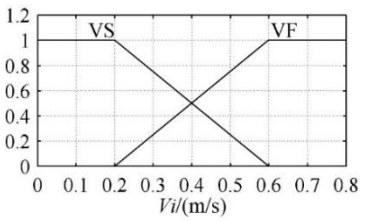

(b) Domain of linear velocity of interfering object

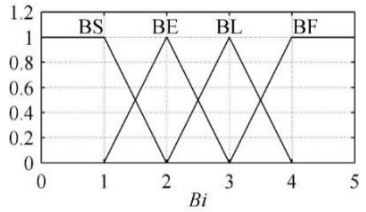

(c) Domain of linear velocity of interfering object

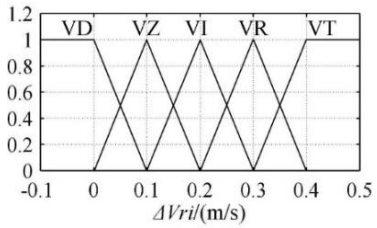

(d) Domain of linear velocity of interfering object

Figure 9 Membership function graph of input/output variable

(2) Fuzzy reasoning

If-then natural sentences based on expert experience and knowledge establish a fuzzy rule library for the above four modes of behavior rules. Fuzzy reasoning takes the input language as the premise and searches for the optimal conclusion in the rule base, the Table 1 shows part fuzzy control rules formulated.

(3) Defuzzification of output variables

The result obtained by fuzzy control rules is a fuzzy quantity, but in actual fuzzy control, the fuzzy quantity cannot directly control the actuator, and it needs to be converted into a precise quantity. Use Mandani reasoning method to get the mean value, as in Eq. (14).

$$\Delta V_{RO}=\frac{\Sigma_{i=1}^{n}\mu(\Delta V_{R_i})\Delta V_{R_i}}{\Sigma_{i=1}^{n}\mu(\Delta V_{R_i})}, \tag{14}$$

Among them, $\Delta V_{RO}$is the calculated robot linear velocity increment, and $\mu(\Delta V_{R_i})$is the membership function value corresponding to the *i* element.

Table 1 Fuzzy control rule (part)

	man-machine distance				Linear velocity		Interference behavior pattern				Linear velocity increment				
i	DS	DE	DN	DF	VS	VF	BS	BE	BL	BF	VD	VZ	VI	VR	VT
1	√				√		√				√				
2	√					√	√				√				
3		√			√			√					√		
4		√				√		√				√			
5			√		√				√					√	
6			√			√			√				√		
7				√	√					√					√
8				√		√				√					√

(4) Simulation and experiment

The simulation analysis mainly considers the two basic behavior patterns of human (interfering object) movement, crossing and encountering mode, and randomly sets the position of human relative to the robot, the starting and ending movement points according to the behavior pattern. The trajectory of the hollow circle represents the trajectory of the robot, and the trajectory of the solid square represents the human walking route. In order to make the simulation results clear and convenient to mark the reference line, pre-set the motion trajectory of the robot as a straight line, the path points are sampled and analyzed with 1s as the unit. Simulations and experiments are not limited to the experimental parameters used in the design, the speed of the robot and human also can be modified as needed.

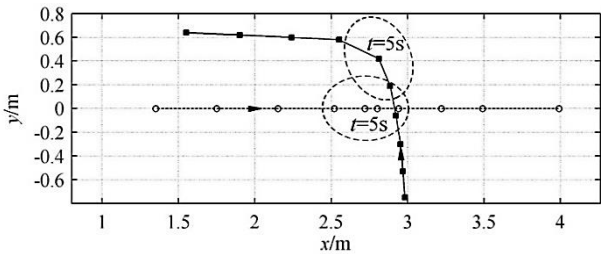

Figure 10 Trajectory simulation of robots and human obstacles in crossing behavior mode

As shown in Figure 10, the simulation experiment 1 was considered the common crossing behavior at the intersection. In this case, the interfering object moved along the set movement route at an initial speed of 0.4 m/s, and the robot

performed a constant-speed inspection work at an initial speed of 0.4 m/s. At t=4.2s, the robot detected that an interfering object entered the maximum avoidance distance area from the right side of the robot moving direction, the robot speed adopted a speed reduction strategy to produce 75% of the initial speed, 0.3 m/s. At t=5.5s, the speed dropped to the lowest, 0.1 m/s. As shown in Figure 11, at t=7.6s, the interfering object left the maximum avoidance area and accelerated to the initial speed, 0.4m/s. The elliptical social distance analysis result of the two sampling points at t=5s shows that when the robot meets with human, exists overlapping phenomenon in sensitive areas.

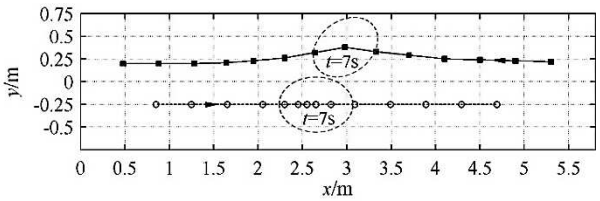

Figure 11 Speed change trend of the robot in crossing behavior mode

In the algorithm experiment under the crossing behavior mode, the initial distance between the human and the robot was kept at the about 5m, and the experimenter crossed from the front left of the robot to the right, and the speed was similar to the robot, as shown in Figure 12(a). At about 5s, the robot started to decelerate and wait. At this time, the distance between human and machine measured by the ultrasonic sensor was equal to the avoidance distance of the robot, as shown in Figure 12(b). When a person passed and left, the distance between the man and the robot detected by the robot increased, its speed accelerated, and finally it detected that it entered the interference area with the front wall until judged that the dangerous distance and stopped.

(a) Approach robot (b) Robot decelerate to avoid (c) Human leave

Figure 12 Experiment of crossing behavior

The simulation experiment 2 was considered the common encountering behavior mode in the aisle. As shown in Figure 13, when the robot inspection strategy was based on the premise that the inspection route does not change, the walking route of the tester could be set as needed. The obstacle movement speed was 0.4 m/s, and the robot movement speed was 0.4 m/s. As shown in Figure 14, at t=4.2s, the robot detected that an intervener entering the maximum avoidance distance area from the left side of the robot moving direction, and the robot speed adopted a speed reduction strategy. At t=6.8s, the speed dropped to the minimum, 0.1m/s. At t=9.3s, the intervener left and the robot accelerated to the original speed.

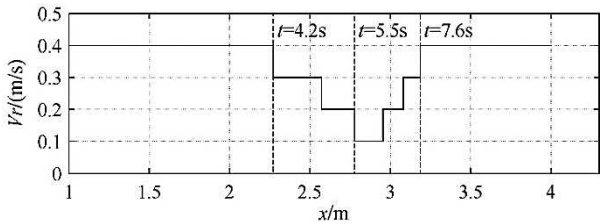

Figure 13 Simulation of the robot and human obstacle trajectory in encountering behavior mode

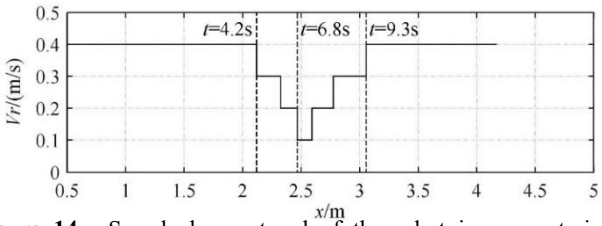

Figure 14 Speed change trend of the robot in encountering behavior mode

As shown in Figure 15(a), in the encountering behavior mode algorithm experiment, the initial distance between the human and the robot was kept at about 8m, and the experimenter approached from the front of the robot to the right side, and the speed was similar to the robot. As shown in Figure 15(b), at about 4s, the robot started to decelerate and wait. At this time, the distance between human and robot measured by the ultrasonic sensor was equal to the avoidance distance of the robot. Finally, the person gradually left, the distance between the man and the robot detected by the robot increased, and the robot movement speed gradually increased to the initial speed. From the two experimental results, the robot realized obstacle avoidance under the original trajectory smoothly.

(a) Approach robot (b) Enter the interactive space (c) Human leave
Figure 15 Experiment of encountering behavior

Through the crossing and encounter interference behavior experiments, it is verified that the dynamic avoidance strategy under the fuzzy logic proposed can make the robot produces matching avoidance behaviors according to the expected obstacle avoidance strategy under the two interference situations and successfully avoid collision with human. The experimental results shows that the obstacle avoidance strategy of the robot is fast responsive, and the small-scale time delay of the speed change does not affect the obstacle avoidance effect. Additionally, when the robot moves in a human environment, the robot and the human will always maintain a sufficient safe distance to reduce the "sense of crisis" produced by human towards to the robot.

5.2 Autonomous Tracking Strategy of the Robot

Robot autonomous tracking strategy is one of the robot most important functions, it relates to the efficiency of the hazardous gas inspection robot. Consider the robot target job requirements, its expected tracking route is drew in advance, combines the obstacle avoidance strategy proposed above, Fuzzy-PID method to control is adopted.

5.2.1 Modeling

Based on the analysis and calculation above, the kinematic model of the robot can be got. The vector $\xi_1=[x, y, \theta]^{\mathrm{T}}$ is the robot position vector, v, ω, θ are the robot speed, angular velocity and rotation angle, respectively. The vector $\xi_{\mathrm{r}}=[x_{\mathrm{r}}, y_{\mathrm{r}}, \theta_{\mathrm{r}}]^{\mathrm{T}}$ is the target position vector of the robot. v_{r}, ω_{r}, θ_{r} represent the target speed velocity, target angular velocity and target rotation angle of the robot, respectively. Vector $\xi_{\mathrm{e}}=[x_{\mathrm{e}}, y_{\mathrm{e}}, \theta_{\mathrm{e}}]^{\mathrm{T}}$ is the robot position error vector. v_{e}, ω_{e}, θ_{e} are the errors of robot speed, angular speed and rotation angle, respectively.

The robot coordinate error is:

$$\xi_{\mathrm{e}}=\begin{bmatrix} x_{\mathrm{e}} \\ y_{\mathrm{e}} \\ \theta_{\mathrm{e}} \end{bmatrix}=\begin{bmatrix} \cos\theta_{\mathrm{r}} & \sin\theta_{\mathrm{r}} & 0 \\ -\sin\theta_{\mathrm{r}} & \cos\theta_{\mathrm{r}} & 0 \\ 0 & 0 & 1 \end{bmatrix}\begin{bmatrix} x-x_{\mathrm{r}} \\ y-y_{\mathrm{r}} \\ \theta-\theta_{\mathrm{r}} \end{bmatrix}, \tag{15}$$

Differential form of position error is:

$$\begin{cases} \mathrm{d}x_{\mathrm{e}}=\omega_{\mathrm{r}} y_{\mathrm{e}}+v\cos\theta_{\mathrm{e}}-v_{\mathrm{r}} \\ \mathrm{d}y_{\mathrm{e}}=-\omega_{\mathrm{r}} x_{\mathrm{e}}+v\sin\theta_{\mathrm{e}} \\ \mathrm{d}y_{\mathrm{e}}=\omega_{\mathrm{r}}-\omega \end{cases}, \tag{16}$$

In order to make the errors as small as possible, designs the auxiliary kinematics controller based on the robot position error vector:

$$\begin{bmatrix} v \\ \omega \end{bmatrix}=\begin{bmatrix} v_{\mathrm{r}}\cos\theta_{\mathrm{e}}+k_1 x_{\mathrm{e}} \\ \omega_{\mathrm{r}}+k_2 v_{\mathrm{r}}\sin\theta_{\mathrm{e}}+k_3 v_{\mathrm{r}} y_{\mathrm{e}} \end{bmatrix}, \tag{17}$$

k_1, k_2, k_3 are different auxiliary control parameter respectively, and under these auxiliary control rates, v, ω gradually converges to v_{r}, ω_{r}. After getting the linear velocity and angular velocity of the robot, angular speed of driving wheel ω_1, ω_2 can be solved through the kinematic equation.

$$\begin{cases} \omega_1=(v+\frac{1}{2}\omega L)/r \\ \omega_2=(v-\frac{1}{2}\omega L)/r \end{cases}, \tag{18}$$

Assume angular speed error of driving wheel ω_{e} = e(t), using PID controller, the controller output u(t) can be got [29].

$$\mathrm{u}(t)=K_{\mathrm{p}}\mathrm{e}(t)+K_{\mathrm{i}}\int \mathrm{e}(t)\mathrm{d}t+K_{\mathrm{d}}\frac{\mathrm{de}(t)}{\mathrm{d}t}, \tag{19}$$

Since the position error generally exists, the team set a range for the deviation distance, $[-l, l]$, then set the fuzzy controller from the control toolbox in the MATLAB/Simulink software to design the fuzzy controller, and respectively to formulate the input and output control rules，as shown in Figure 16.

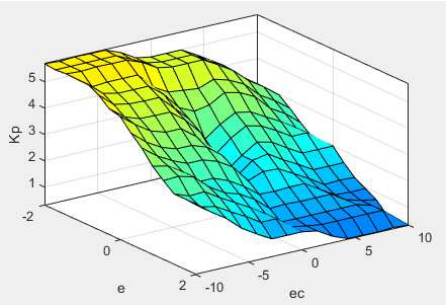

(a) K_p

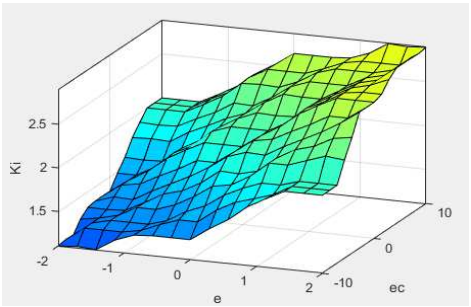

(b) K_i

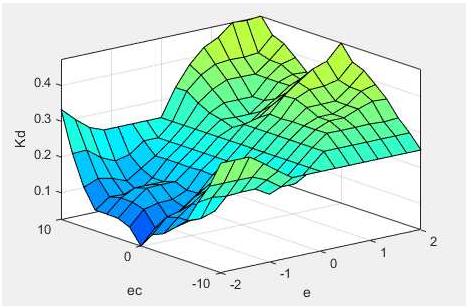

(c) K_i

Figure 16 Output surfaces of K_p, K_i, K_d

The second step was to utilize the membership function in different ranges to solve K_p, K_i, K_d [30]. The specific control method was presented in the Figure 17.

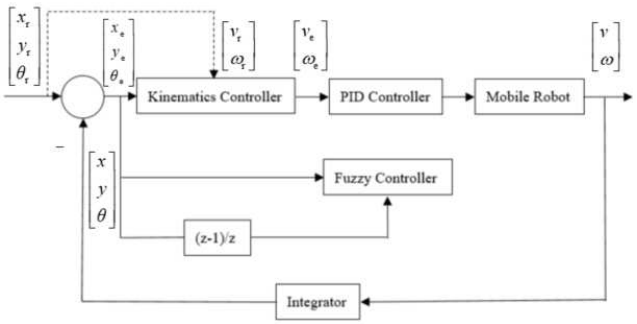

Figure 17 Motion controller of the robot

5.2.2 Simulation and Experiments

In order to verify the effectiveness of the controller, the robot was tested in an indoors man-machine environment. First drew a circular trajectory on the floor as the target trajectory, then placed the robot at a distance from the target trajectory.

Figure 18 Target trajectory of the robot

The robot target trajectory as shown in Figure 18. The robot experiment platform also includes a PC host, which installs with control software and camera processing software to track the robot trajectory and generate trajectory map, as Figure 19 shows. The target of the robot starting point is (3.5, 0). The Initial position error is (0.2, -0.5) and the initial angle error is $\pi/6$.

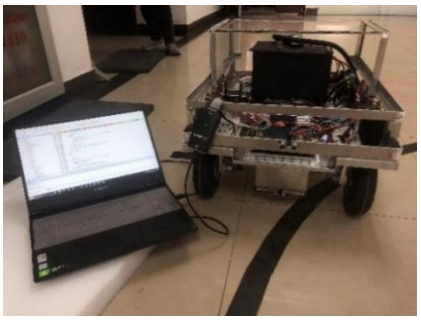

Figure 19 Experiment platform of the robot

In the robot, the PTZ is a two-degree-of-freedom double-headed device that can rotate 0−360° horizontally and freely swing -90°−90° vertically. The PTZ and the movement mechanisms of the robot are independent of each other, and the PTZ patrol action group can be set as required. The monitoring range is wide, the monitoring posture change is more flexible and possesses certain shock absorption and explosion-proof functions, which can improve the stability of monitoring equipment. The robot is equipped with Hikvision DS-2ZMN3007 network high-definition camera with 2 million pixels, and the resolution is up to 1920*1080, small size and low power consumption are more suitable to

the inspection of the robot. The camera used to detect dangerous gases chooses FLIR gas thermal imager G300a, which can visualize the distribution of leaked gas and lock its leak position. The leaked gas can be detected at a safe distance through non-contact mode, and it can also facilitate scanning the detection areas that are inaccessible by traditional inspection method.

For real-time video transmission, the robot adopts a C/S architecture and makes the robot as a streaming media server. Under the framework of the open source video server Mjpg-streamer, the video information collected from the camera is encoded and sent to remote client, monitoring terminal as a network client receives video data from the server, and displays the process in the upper computer window after the video is decoded. Because the open source video server Mjpg-streamer framework uses M-JPEG image compression technology to compress video frame by frame, the compression efficiency is low, and smooth video transmission cannot be achieved in a bandwidth-constrained network. Therefore, after the camera image data is collected, the image data needs to be H.264 hard-coded, compressed into a video image in H.264 format to make the size and format of the image meet the needs of video transmission. Finally the UDP protocol is selected on the transport layer to improve the video transmission efficiency and improve the video delay problem. Consequently, the image transmission speed can reach 10 frames per second and the transmitted images have good real-time performance, the visible light video and thermal imaging video can be displayed in real time through the upper computer software designed by the team. As shown in Figure 20, when the robot is moving and its speed changes, the PTZ is stable, and the real-time image obtained is clear.

(a) Display of the real time visible light video

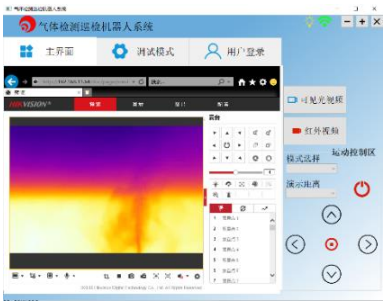

(b) Display of the real time thermal imaging video

Figure 20 Display the real time video of the robot inspection

Processed the robot motion in tracing experiments, when the robot detects a static obstacle wall in a turning state, it can be seen from Figure 21 that the robot will slowly decelerate to the nearest speed after smoothly passing the wall, and the actual trajectory of mobile robot movement was as shown in Figure 22. When the robot walked 1/4 of the circle, recorded the coordinate position of the robot, as shown in Table 2. Analysis the robot motion data, the robot position error (coordinate unit: meter) and rotation angle error can be calculated respectively.

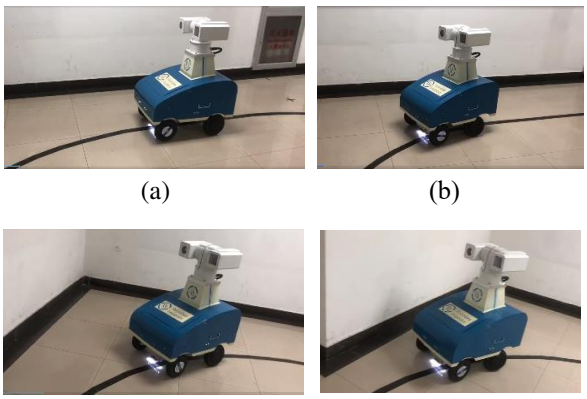

(a) (b)

(c) (d)

Figure 21 Tracking experiment the robot

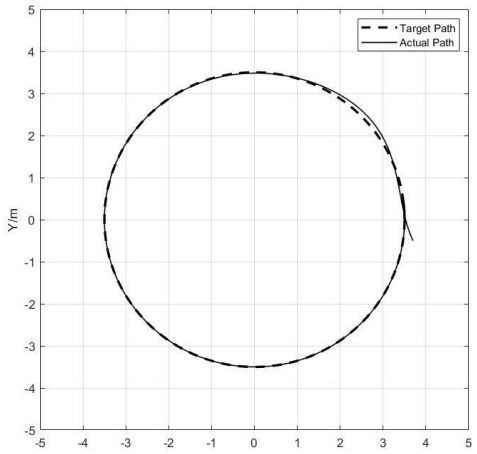

Figure 22 Actual trajectory of the robot

Table 2 Expected and actual positions of each point m

Coordinate points	Target point	Actual point
1	(0, 3.5)	(0.003, 3.482)
2	(-3.5, 0)	(-3.497, 0.015)
3	(0, -3.5)	(0.018, -3.49)
4	(3.5, 0)	(3.499, 0.008)

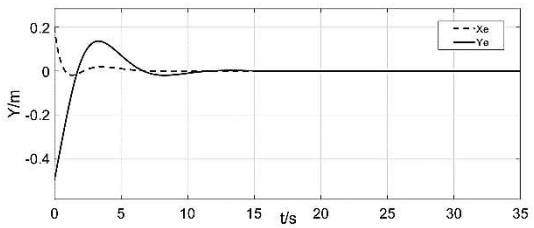

Figure 23 Position error the robot

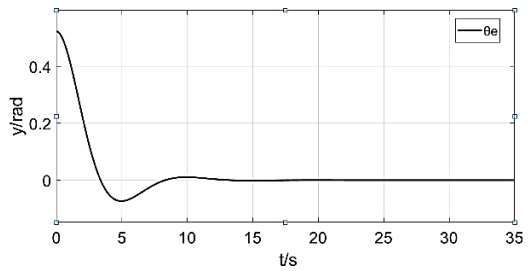

Figure 24 Angle error of the robot

The experimental results show that when the robot deviates from the predetermined position, the motion controller can help the robot return to the original track more quickly. When the robot runs the smoothly, it can complete the inspection of target tracking indoors well, control the position error up to 10mm and angle error up to 0.1 rad. And when robot is running, it can transmit back the environmental and gas inspection image information timely and efficiently.

6 Conclusions

(1) Based on the research of the mobile robot to inspect hazardous gas, this research designs a mobile inspection robot, builds the kinematic model of the robot, establishes a hybrid architecture of the control system to improve the rapid responsiveness of the system and get the overall coordination and decision-making abilities.

(2) In the dynamic and time-varying environment which shared space between humans and machines, the team analyzes human movement and behavior and divides them into four typical behavior patterns to describe with fuzzy language, establishes a social force model that matches the environment based on the human mental state. Based on social force model and fuzzy logic, proposes an inspection method for mobile dynamic obstacle avoidance.

(3) With sets of the crossing mode and encountering mode simulation and experiments, the obstacle avoidance performance of the robot is taken, the small-scale time delay of the speed change does not affect the obstacle avoidance effect, the robot and the human will always maintain a sufficient safe distance to reduce the "sense of crisis" produced by human towards to the robot.

(4) Combine the dynamic obstacle avoidance strategy presents an autonomous tracking strategy controlled by Fuzzy-PID control system. The trajectory experiments results are similar to the simulation, verifies that when the hazardous gas inspection robot deviates from the predetermined trajectory, the robot can return to the original trajectory, and control the position error to 10mm and angle error up to 0.1 rad. Besides, the PTZ can rotate 0−360° horizontally and freely swing -90°−90° vertically. The inspection of the robot is more flexibility since the PTZ is independent with the movement mechanisms of the robot, and the PTZ patrol action group can be set as required. The robot can transmit back the image information timely and efficiently, the image transmission speed can reach 10 frames per second, and the image is clear regardless of the movement state of the robot moving mechanism. In summary, the results show that the combination moving strategy presented in this paper is effective and practical, can more reliably protect the safety of robots and humans and the robot can complete the task of hazardous gas inspection well in complex man-machine environment.

7 Declaration

Acknowledgements

The authors sincerely thanks to *Xi'an Modern Chemistry Research Institute for their supports.*

Funding

Supported by Research and Development Program of *Xi'an Modern Chemistry Research Institute* (Grant No. 204J201916234/6).

Availability of data and materials

The datasets supporting the conclusions of this article are included within the article.

Authors' contributions

The author' contributions are as follows: XG was in charge of the whole trial; QZ wrote the manuscript; XG, BL, XF and JL assisted with sampling and laboratory analyses. All authors read and approved the final manuscript.

Competing interests

The authors declare no competing financial interests.

Consent for publication

Not applicable

Ethics approval and consent to participate

Not applicable

References

[1] FG Pratticò, F Lamberti. Mixed-reality robotic games: design guidelines for effective entertainment with consumer robots. *IEEE CONSUMER ELECTRONICS MAGAZINE*, 2021, 10(1): 6-15.

[2] DY Huang, CG Yang, YP Pan, et al. Composite learning enhanced neural control for robot manipulator with output error constraints. *IEEE TRANSACTIONS ON INDUSTRIAL INFORMATICS*, 2021, 17(1):209-218.

[3] T Yang, XS Gao, FQ Dai. New hybrid AD methodology for minimizing the total amount of information content: a case study of rehabilitation robot design. *CHINESE JOURNAL OF MECHANICAL ENGINEERING*, 2020, 33(1).

[4] W Zhang, SL Wei, YB Teng, et al. Dynamic obstacle avoidance for unmanned underwater vehicles based on an improved velocity obstacle method. *SENSORS*, 2017, 17(12).

[5] J Lopez, P Sanchez-Vilarino, MD Cacho, et al. Obstacle avoidance in dynamic environments based on velocity space optimization. *ROBOTICS AND AUTONOMOUS SYSTEMS*. 2020, 131.

[6] Y Chen, JD Han, HY Wu. Quadratic programming-based approach for autonomous vehicle path planning in space. *CHINESE JOURNAL OF MECHANICAL ENGINEERING*, 2012, 25(4): 665-673.

[7] T Lv, M Feng. A smooth local path planning algorithm based on modified visibility graph. *MODERN PHYSICS LETTERSB*, 2017, 31(19-21).

[8] E Ferrera, J Capitan, AR Castano, et al. Decentralized safe conflict resolution for multiple robots in dense scenarios. *ROBOTICS AND AUTONOMOUS SYSTEMS*, 2017, 91:179-193.

[9] MP Polverini, AM Zanchettin, P Rocco. A computationally efficient safety assessment for collaborative robotics applications. *ROBOTICS AND COMPUTER-INTEGRATED MANUFACTURING*, 2017, 46: 25-37.

[10] R Singh, TK Bera. Walking model of Jansen Mechanism-based quadruped robot and application to obstacle avoidance. *ARABIAN JOURNAL FOR SCIENCE AND ENGINEERING*, 2020, 45(2): 653-664.

[11] N Takahashi, N Shibata, K Nonaka. Optimal configuration control of planar leg/wheel mobile robots for flexible obstacle avoidance. *CONTROL ENGINEERING PRACTICE*, 2020, 101.

[12] Khatib O. Real-time obstacle avoidance for manipu-lators and mobile robots. *The International Journal of Robotics Research*, 1986, 5(1): 90-98.

[13] CT Diao, SM Jia, GL Zhang, et al. Design and Realization of a Novel Obstacle Avoidance Algorithm for Intelligent Wheelchair Bed Using Ultrasonic Sensors. *2017 CHINESE AUTOMATION CONGRESS* (CAC), 2017: 4153-4158.

[14] J. A Janet, R. C Luo, M. G Kay. The Essential Visibility Graph: an approach to global motion planning for autonomous mobile robots. 1995 *IEEE International Conference on Robotics and Automation*, 1995, 2: 1958-1963.

[15] L Blasi, E D'Amato, M Mattei, et al. Path planning and real-time collision avoidance based on the Essential Visibility Graph. *APPLIED SCIENCES-BASEL*, 2020, 10(16).

[16] l Ulrich, J Borenstein. VFH*: local obstacle avoidance with look-ahead verification. *2002 IEEE International Conference on Robotics and Automation*, 2000:24-28.

[17] XY Li, F Liu, J Liu, et al. Obstacle avoidance for mobile robot based on improved dynamic window approach. *TURKISH JOURNAL OF ELECTRICAL ENGINEERING AND COMPUTER SCIENCES*, 2017, 25(2): 666-676.

[18] PK Mohanty. An intelligent navigational strategy for mobile robots in uncertain environments using smart cuckoo search algorithm. *JOURNAL OF AMBIENT INTELLIGENCE AND HUMANIZED COMPUTING*, 2020.

[19] NT Thinh, NT Tuan, LP Huang. Predictive controller for mobile robot based on fuzzy logic. *2016 3RD INTERNATIONAL CONFERENCE ON GREEN TECHNOLOGY AND SUSTAINABLE DEVELOPMENT* (GTSD), 2016: 141-144.

[20] YL Fu, SG Wang, ZC Cao. Behavior-based robot fuzzy motion planning approach in unknown environments. *CHINESE JOURNAL OF MECHANICAL ENGINEERING*, 2006, 42(5): 120-125.

[21] XY Li, N Xu, Q Li, et al. A fusion methodology for sideslip angle estimation on the basis of kinematics-based and model-based approaches. *PROCEEDINGS OF THE INSTITUTION OF MECHANICAL ENGINEERS PART D-JOURNAL OF AUTOMOBILE ENGINEERING*, 2020, 234(7): 1930-1943.

[22] V Dolk, J den Ouden, S Steeghs, et al. Cooperative automated driving for various traffic scenarios: experimental validation in the GCDC 2016. *IEEE TRANSACTIONS ON INTELLIGENT TRANSPORTATION SYSTEMS*, 2018, 19(4): 1308-1321.

[23] KP Valavanis. The entropy based approach to modeling and evaluating autonomy and intelligence of robotic systems. *JOURNAL OF INTELLIGENT & ROBOTIC SYSTEMS*, 2018, 91(1): 7-22.

[24] GN Saridis, HE Stephanou. A hierarchical approach to the control of a prosthetic arm. *IEEE TRANSACTIONS ON SYSTEMS MAN AND*

CYBERNETICS, 1977, 7(6): 407-420.
[25] CM Ye, J Li, H Jiang, et al. Semi-Automated Generation of Road Transition Lines Using Mobile Laser Scanning Data. *IEEE TRANSACTIONS ON INTELLIGENT TRANSPORTATION SYSTEMS*, 2020, 21(5): 1877-1890.
[26] K Ren, Q Wang, C Wang, et al. The security of autonomous driving: threats, defenses, and future directions. *PROCEEDINGS OF THE IEEE*, 2020, 108(2): 357-372.
[27] A Hacinecipoglu, EI Konukseven, AB Koku. Multiple human trajectory prediction and cooperative navigation modeling in crowded scenes. *INTELLIGENT SERVICE ROBOTICS*, 2020, 13(4): 479-493.
[28] SD Lynch, R Kulpa, LA Meerhoff, et al. Influence of path curvature on collision avoidance behaviour between two walkers. *EXPERIMENTAL BRAIN RESEARCH*, 2020.
[29] JD Han, ZQ Zhu, ZY Jiang, et al. Simple PID Parameter Tuning Method Based on Outputs of the Closed Loop System. *CHINESE JOURNAL OF MECHANICAL ENGINEERING*, 2016, 29(3): 465-474.
[30] HG Mi, HW Yuan, QS Wang. Algorithm Research and Realization of the Turning Control System for Heavy Transportation Vehicle. *CHINESE JOURNAL OF MECHANICAL ENGINEERING*, 2012, 25(3): 530-535.

Biographical notes

Qing-Fang Zhang, born in 1994, is currently a PhD candidate at *Beijing Institute of Technology, China*. Her research interests include mobile robot, intelligent control and intelligent robotics.
Tel: +18801292685; E-mail: 3120195161@bit.edu.cn

Xue-Shan Gao, born in 1966, is currently a professor and a PhD candidate supervisor at *Beijing Institute of Technology, China*. His main research interests include mobile robot, intelligent robotics and medical robot. He is a senior member of *Chinese mechanical Engineering Society* (CMES) and an organizing committee chair of *IEEE International Conference on Mechatronics and Automation* (ICMA) 2020.
E-mail: xueshan.gao@bit.edu.cn

Bing-Qing Lan, born in 1994, is currently a master candidate at *Beijing Institute of Technology, China*.
E-mail: 2319605124@qq.com

Xiao-Long Fu, born in 1982, is currently a researcher at *Xi'an Modern Chemistry Research Institute, China*. His research interests include unmanned monitoring technology and materials science.
E-mail: fuxiaolong204@163.com

Jing-Ye Li, born in 1995. He received his master degree from *Beijing Institute of Technology, China*, in 2020. His research interests include mobile robot technology.
E-mail: lijingye0831@163.com

Appendix

No appendix.

Figures

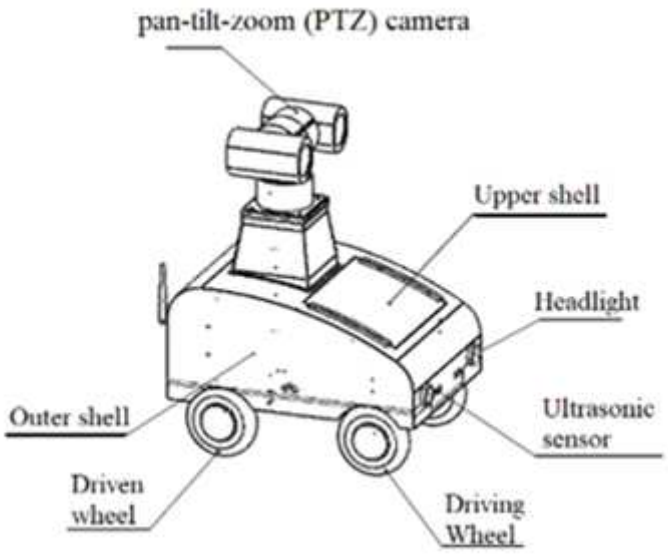

Figure 1

Schematic diagram of the robot overall structure

Figure 2

Prototype of the robot

Figure 3

Moving mechanism of the robot

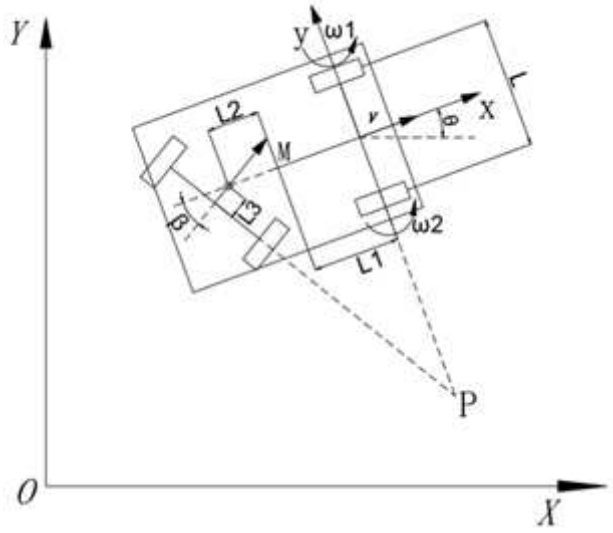

Figure 4

Kinematics model of the robot

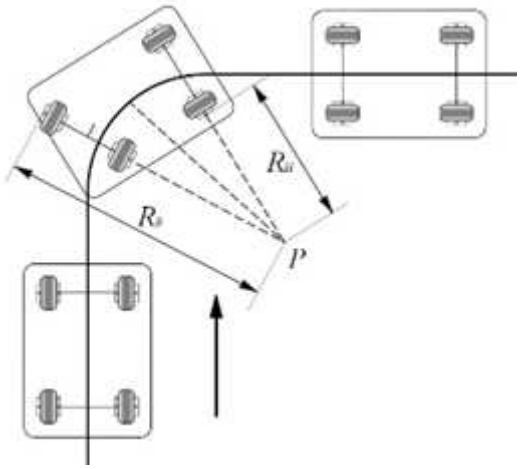

Figure 5

Schematic diagram of the robot turning motion

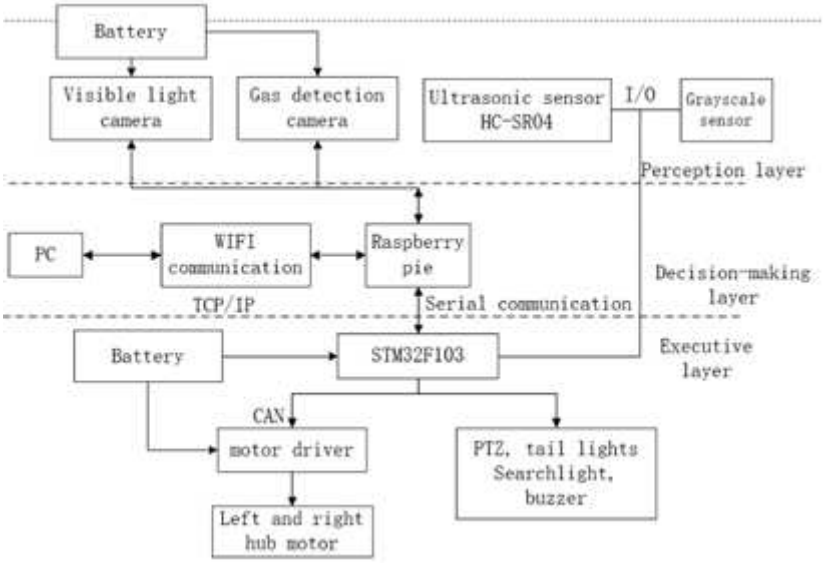

Figure 6

Structure of the robot control system

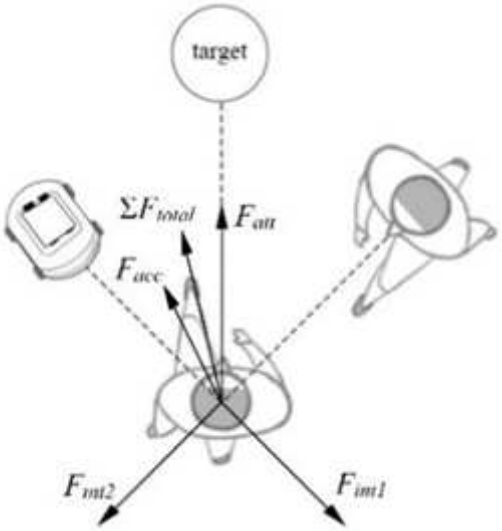

Figure 7

Social power model

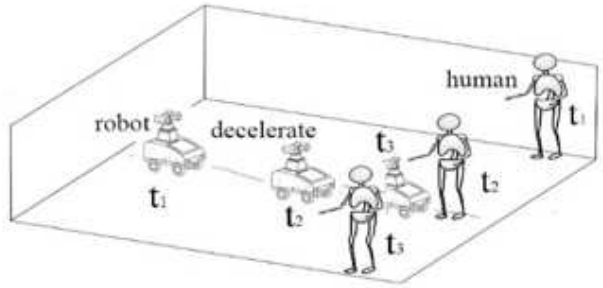

(a) Crossing behavior

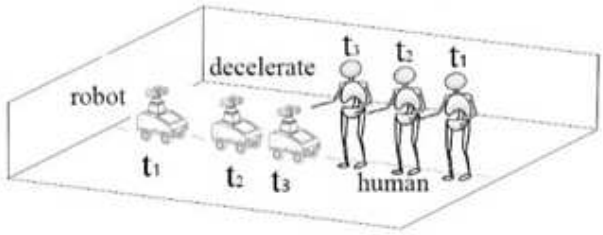

(b) Encountering behavior

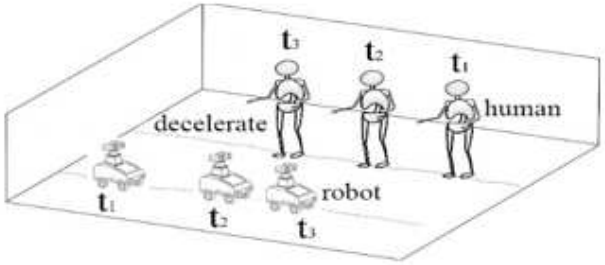

(c) Leading behavior

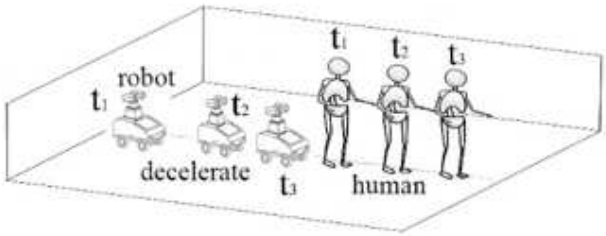

(d) Confronting behavior

Figure 8

Four type of behavior mode

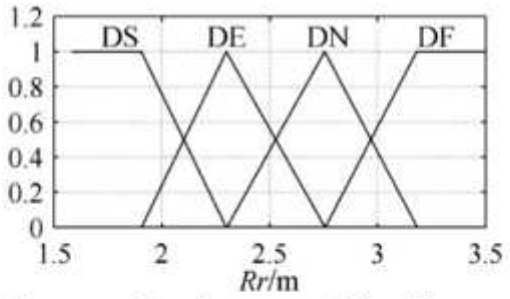

(a) Domain of man-machine distance

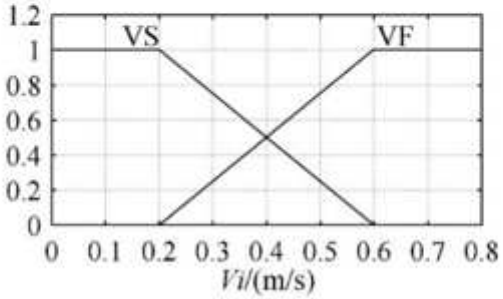

(b) Domain of linear velocity of interfering object

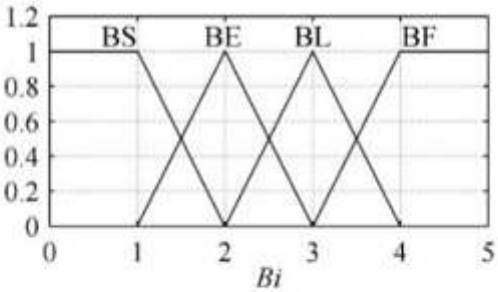

(c) Domain of linear velocity of interfering object

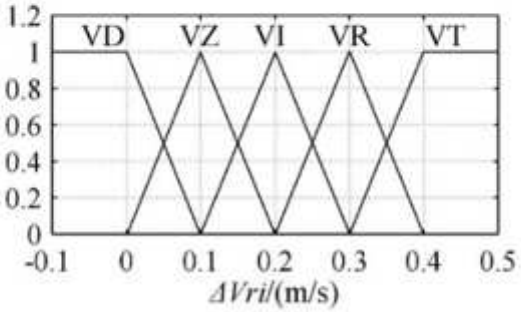

(d) Domain of linear velocity of interfering object

Figure 9

Membership function graph of input/output variable

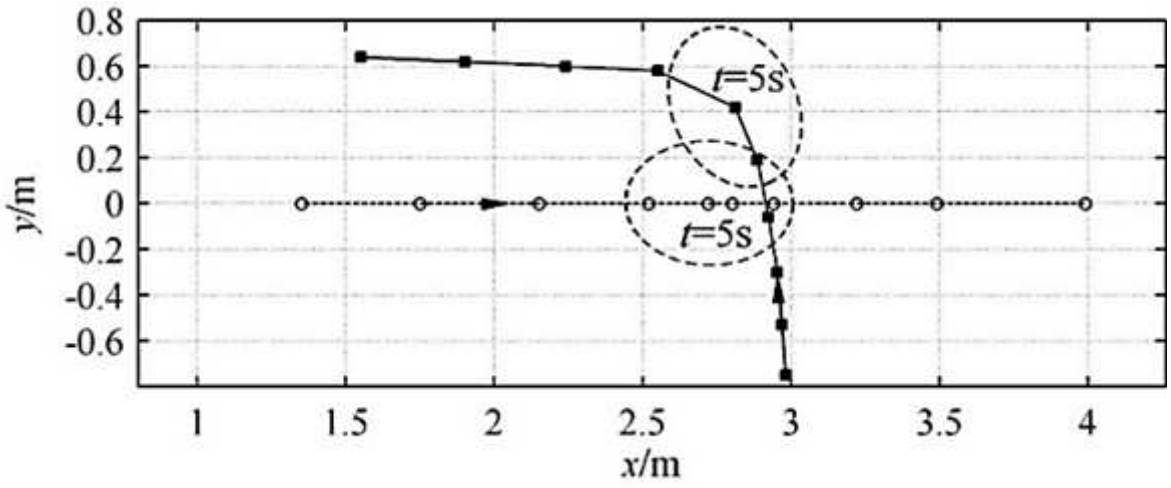

Figure 10

Trajectory simulation of robots and human obstacles in crossing behavior mode

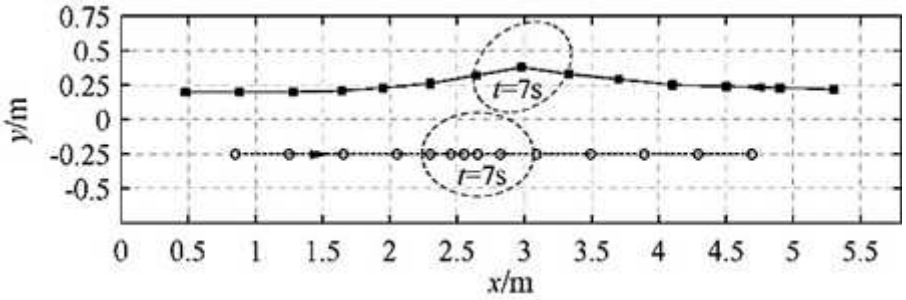

Figure 11

Speed change trend of the robot in crossing behavior mode

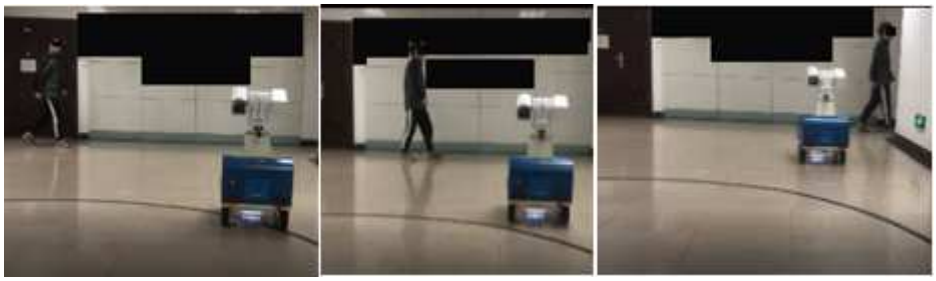

Figure 12

Experiment of crossing behavior

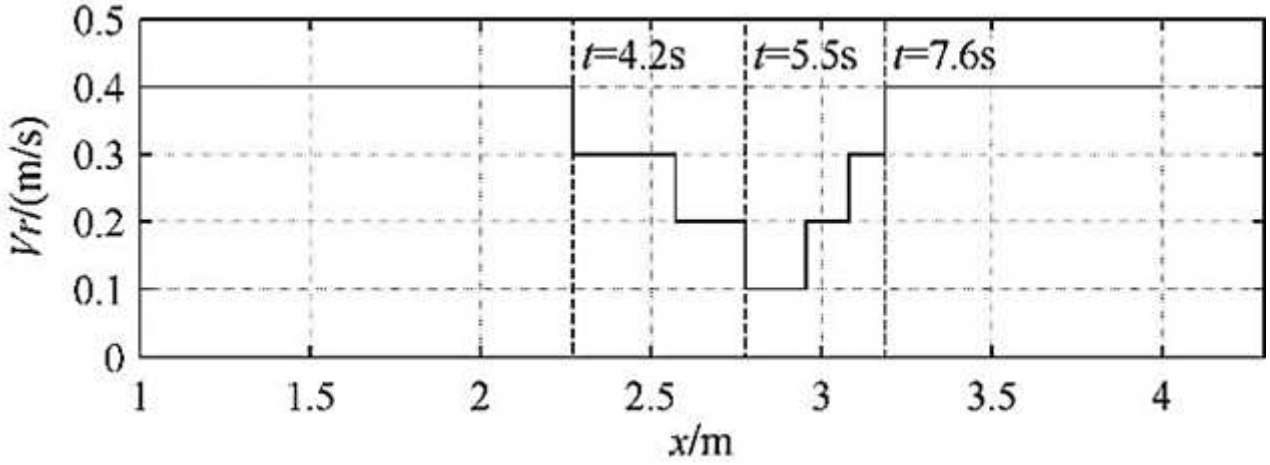

Figure 13

Simulation of the robot and human obstacle trajectory in encountering behavior mode

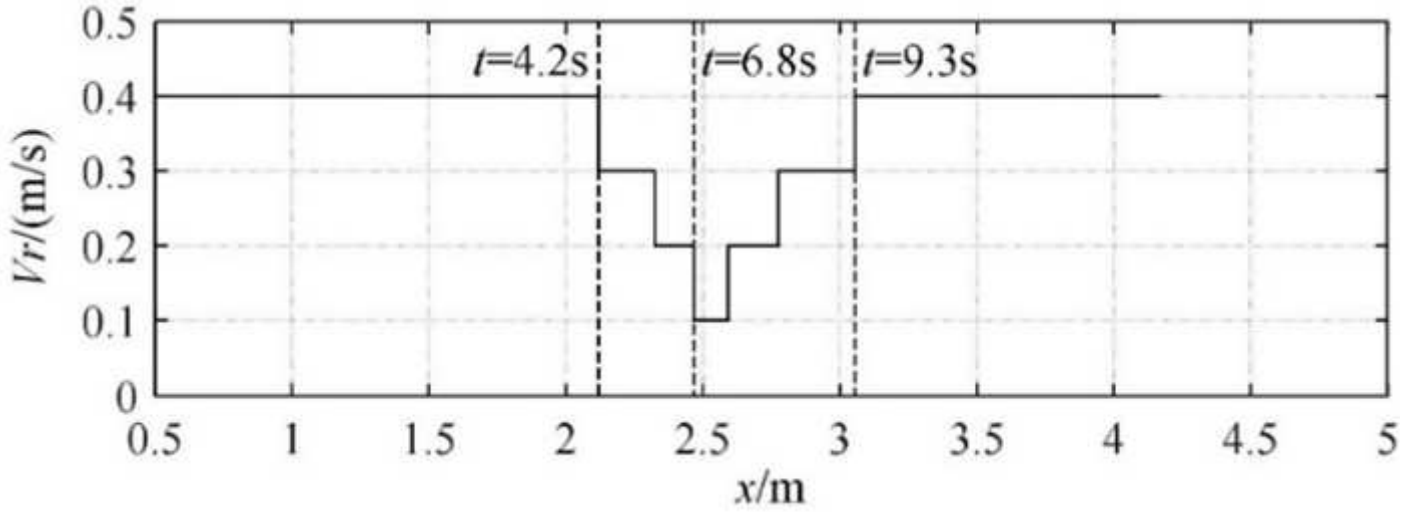

Figure 14

Speed change trend of the robot in encountering behavior mode

(a) Approach robot (b) Enter the interactive space (c) Human leave

Figure 15

Experiment of encountering behavior

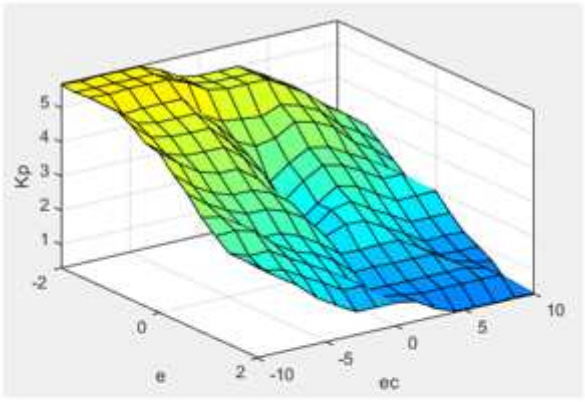

(a) K_p

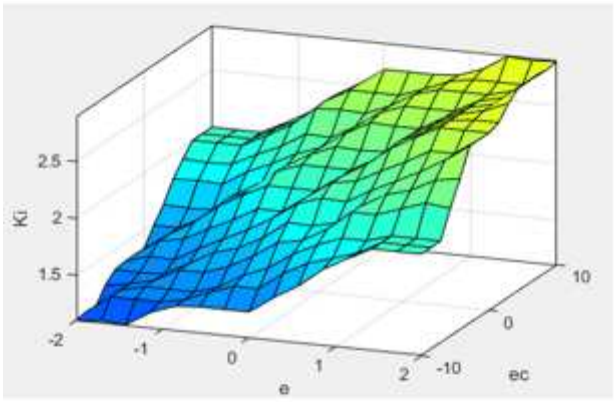

(b) K_i

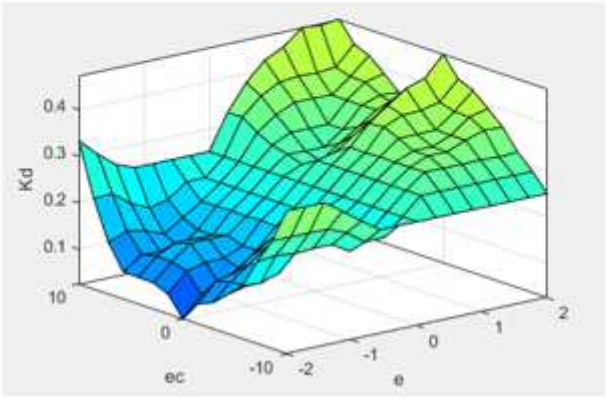

(c) K_i

Figure 16

Output surfaces of Kp, Ki, Kd

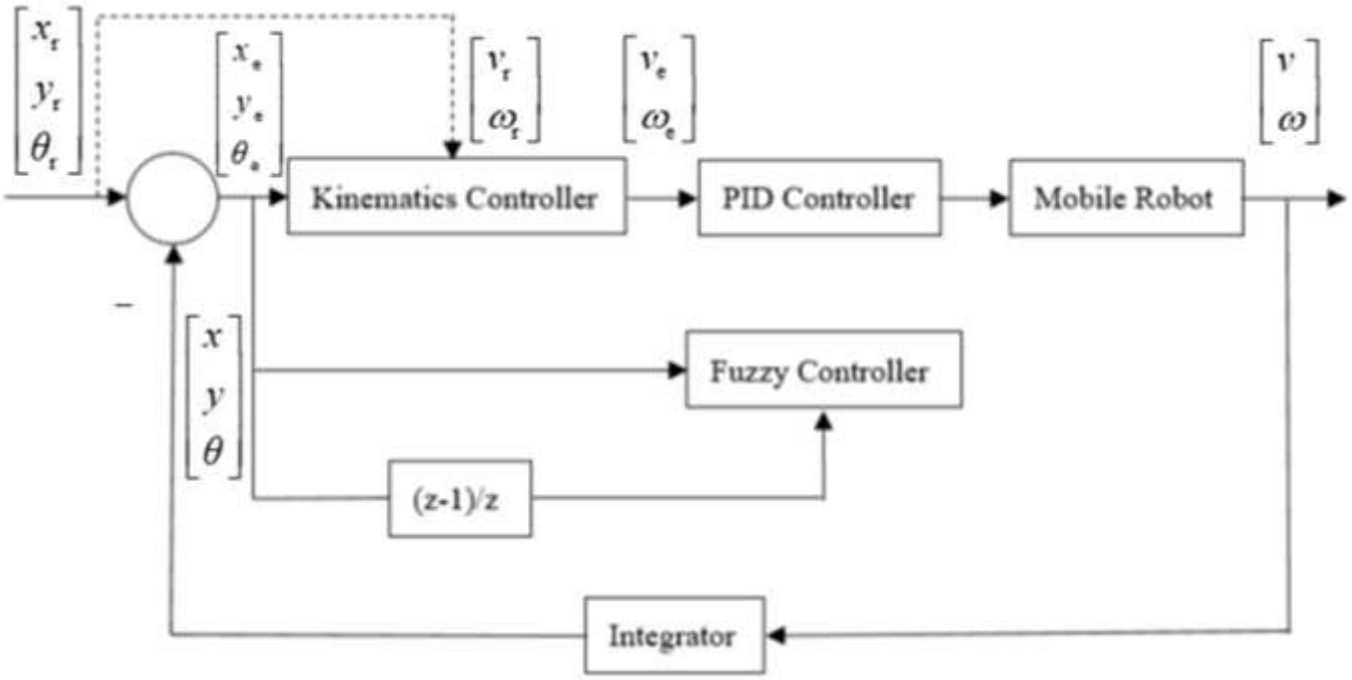

Figure 17

Motion controller of the robot

Figure 18

Target trajectory of the robot

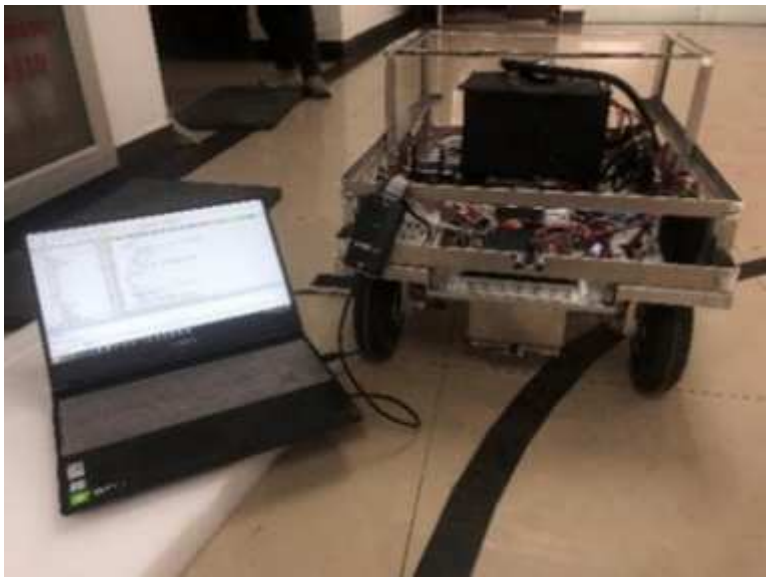

Figure 19

Experiment platform of the robot

(a) Display of the real time visible light video

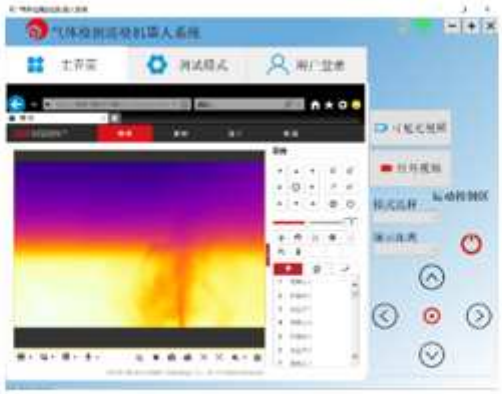

(b) Display of the real time thermal imaging video

Figure 20

Display the real time video of the robot inspection

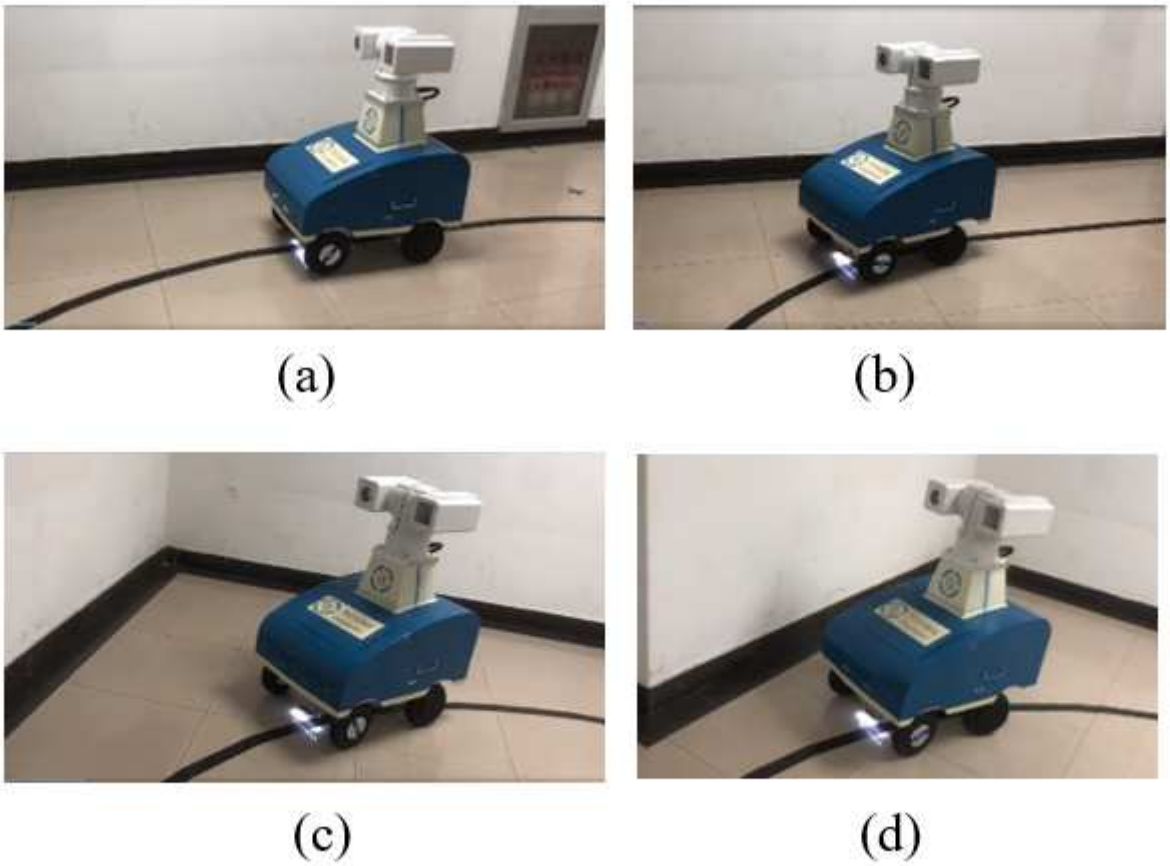

Figure 21

Tracking experiment the robot

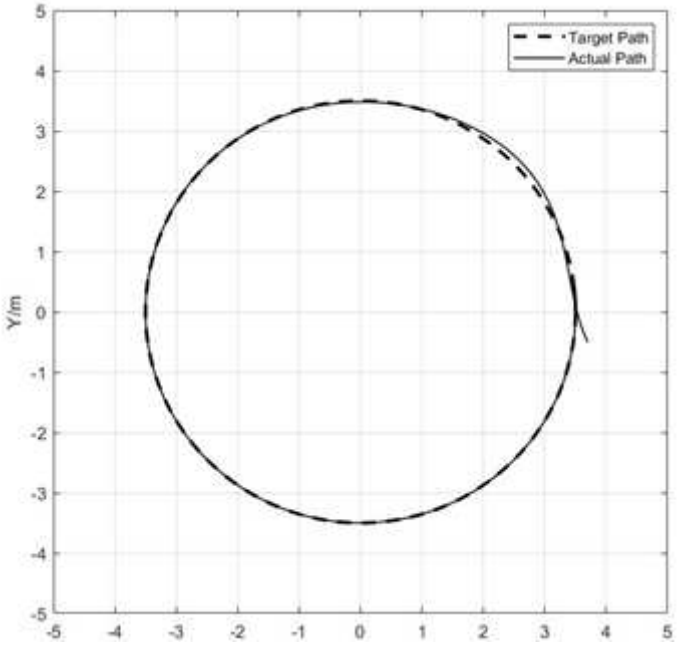

Figure 22

Actual trajectory of the robot

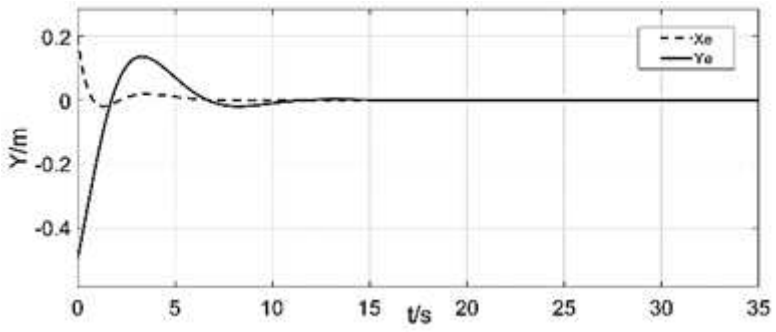

Figure 23

Position error the robot

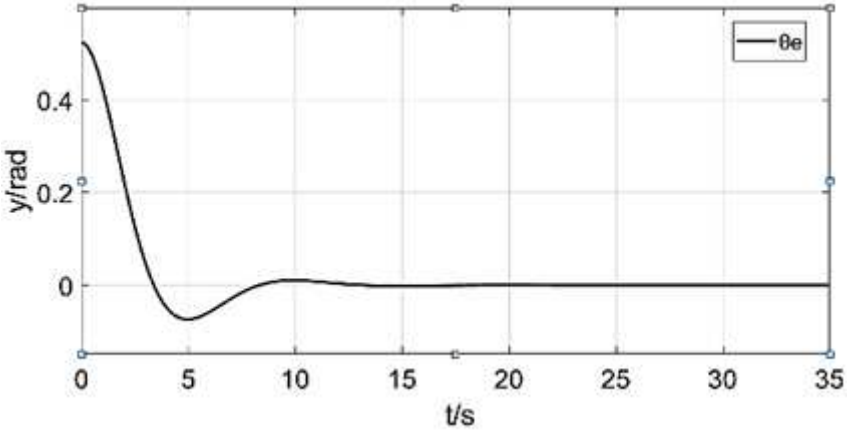

Figure 24

Angle error of the robot